Journal of Sound and Vibration (1999) **223**(4), 543–566
Article No. jsvi.1998.2133, available online at http://www.idealibrary.com on IDEAL®

ANALYSIS OF LOW FREQUENCY ACOUSTIC RESPONSE IN A DAMPED RECTANGULAR ENCLOSURE

J. PAN

Department of Mechanical and Materials Engineering, University of Western Australia, Nedlands, WA 6907, *Australia*

S. J. ELLIOTT AND K.-H. BAEK†

*Institute of Sound and Vibration Research, University of Southampton, Southampton SO*9 5*NH, England*

(*Received* 25 *May* 1998, *and in final form* 30 *November* 1998)

This paper is concerned with the prediction of acoustic response in a well damped rectangular enclosure. The acoustic characteristics of the enclosure are modelled using the modal expansion approach, with suitable modification of the damping and frequency shift introduced into the rigid wall acoustic modes of the enclosure. The prediction of acoustical transfer impedance in the enclosure has demonstrated that a frequency dependent modal parameter may be used to describe the acoustic response. This modal parameter is defined as the specific acoustical modal admittance, which describes the contribution of all the boundaries (locally and modally reactive and air leakage) to the modal damping and the shift of nature frequencies. The sound absorption properties of each boundary type and its effect on the response of the enclosure are analysed. The predicted and measured space-average acoustic transfer impedances in a damped rectangular enclosure are compared and reasonable agreement is found. The Helmholtz resonance effect of the cockpit in a helicopter is also included in the model. The measured dip at about 23 Hz in the space-average acoustic impedance inside the passenger cabin of the helicopter is accurately predicted.

1. INTRODUCTION

The sound pressure inside the passenger cabins of helicopters show a strong component around 15 to 20 Hz, which corresponds to the blade passing frequency (BPF) of the main rotor. Although this noise component is below the lower frequency limit of hearing, it may influence the comfort and performance of passengers. Active noise control techniques have been proposed to attenuate the BPF component and its harmonics [l, 2]. As a preliminary part of an

†Now at Department of Mechanical Engineering, Dankook University, 8, Hannam-Dong, Youngsan-Ku, Seoul, Korea 140-714.

0022–460X/99/240543 + 24 $30.00/0

investigation into this approach, the space-average acoustic impedance inside the passenger cabin of a large helicopter (Agusta-Westlands EH101) was measured and is shown as a solid curve in Figure 12. The space average acoustic impedance is calculated by averaging the modulus of the acoustic impedance measured between a large calibrated acoustic source placed in one corner of the passenger cabin and 12 microphones distributed throughout the enclosure [3]. Numerical simulation has been conducted, which confirms that the average of 12 transfer acoustic impedances can adequately represent the space averaged acoustic impedance in the frequency range of interest. To help understand the characteristics of this transfer impedance, a laboratory enclosure was constructed for detailed analysis. The space-average impedance of the laboratory enclosure is also measured (shown as a solid curve in Figure 3) and can be seen to have similarities at low frequencies with the helicopter space-average impedance. The magnitude of the impedance shows that the enclosure is well damped and that the very low frequency response of the room (below 50 Hz) is unexpectedly low. Even the expected resonance response of the first (0, 1, 0) acoustic mode (at 28 Hz) is not apparent. As a result, difficulties in actively controlling low frequency components using ordinary loudspeakers become apparent as very large inputs to the control loudspeakers might be required to attenuate the primary noise at the low frequencies.

In order to develop an effective method of actively attenuating the low frequency noise components in the enclosures such as that in helicopters, it is necessary to investigate the mechanism of sound absorption by the boundary structures of the enclosure. It is also necessary to study the response of the sound field to airborne excitation by control loudspeakers.

Based on the measured acoustic transfer impedance in the enclosure, this paper presents an analysis of various boundaries and their effect on the room characteristics. A general model of the acoustical response in a room with both locally and non-locally reactive boundaries has been developed. Rigid wall acoustic modes have been used as trial functions of the sound field. Effort has been made to explain the sound absorption by different boundary structures and to derive formulae for the prediction of the low frequency features in the acoustic transfer impedance of the damped rectangular room and helicopter. The model developed provides a base for future analysis of active noise control in such an enclosure.

2. THEORY

2.1. DESCRIPTION OF ENCLOSURE

The acoustic enclosure shown in Figure 1 is made from 24 pieces of plywood panels (approximately $2{\cdot}1 \times 1{\cdot}05 \times 0{\cdot}02$ m^3). The internal dimensions of the enclosure are $L_x = 2{\cdot}1$ m, $L_y = 6{\cdot}0$ m and $L_z = 2{\cdot}1$ m. The floor of the enclosure is covered by a thin layer of carpet on plywood panels backed by the concrete floor of a larger room. The surfaces of three side walls ($x = 0$, $x = L_x$ and $y = L_y$) have been treated by a layer of sound absorption material ($t_a = 0{\cdot}025$ m) and an

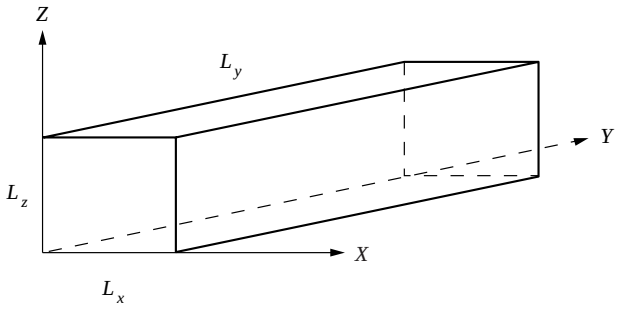

Figure 1. The co-ordinates of the acoustic enclosure.

air gap ($t_g = 0{\cdot}025$ m) is left between the materials and the plywood panels. The ceiling and one of the side walls ($z = L_z$ and $y = 0$) are simple plywood panels ($t_p = 0{\cdot}02$ m). Possible air leakage exists at the joints of the panels. On the side wall $y = 0$, there is a hole ($0 \leqslant x \leqslant 0{\cdot}16$ m and $0 \leqslant z \leqslant 0{\cdot}01$ m) for the cables in and out of the enclosure. In the measurement the loudspeaker was located at one corner of the room (0, L_y 0).

Because low frequency behaviour of the sound field in the enclosure is the object of the present analysis, the modal approach will be used to describe the sound pressure field and the vibration of the boundary structures. An approximate solution of the sound field in an enclosure using rigid wall modes has been developed by Dowell *et al.* [4] by using the Green's identity relationship. In this paper, an alternative approach is used to model the forced response of the sound field in the enclosure on the bases of the modified method of weighted residuals [5]. The same form of the modal coupling equations as that obtained by Dowell *et al.* has been obtained, when rigid wall modes were selected as a set of "convenient" admissible functions in a linear representation of the sound pressure field. It has been shown that to achieve a reasonable convergence of the system response, a large number of rigid wall modes have to be used.

The complex acoustic pressure $p(\mathbf{r})$ in the enclosure is described by the frequency domain acoustic wave equation:

$$(\nabla^2 + k^2)p(\mathbf{r}) = -j\rho_o\omega q(\mathbf{r}), \tag{1}$$

where ρ_o is the air density, k and ω are respectively the wavenumber and angular frequency of the sound waves and $\mathbf{r}$ is the position vector. $q(\mathbf{r})$ is the strength of the sound source describing the volume velocity per unit volume. If the acoustic pressure field is described by the trial solution $p^{(N)}(\mathbf{r})$, the residual of equation (1) can be defined as:

$$R(p^{(N)}(\mathbf{r})) = (\nabla^2 + k^2)p^{(N)}(\mathbf{r}) + j\rho_o\omega q(\mathbf{r}). \tag{2}$$

A set of shape functions $\phi_J(\mathbf{r})$, where $J = 1, 2, \ldots, N$, may now be selected to represent the spatial variation of the pressure field. Imposing the condition that they are all orthogonal to the residual (i.e., $\int_V \phi_J(\mathbf{r})R(p^{(N)}(\mathbf{r}))\,\mathrm{d}v = 0$), the

following equation can be derived for each $\phi_J(\mathbf{r})$:

$$\int_V \phi_J(\mathbf{r})\nabla^2 p^{(N)}(\mathbf{r})\ \mathrm{d}v + k^2 \int_V \phi_J(\mathbf{r}) p^{(N)}(\mathbf{r})\ \mathrm{d}v = -j\rho_o\omega \int_V q(\mathbf{r})\phi_J(\mathbf{r})\ \mathrm{d}v. \tag{3}$$

In case the trial solution does not satisfy the natural boundary conditions of the enclosure, the interaction between the boundary and sound field should be included in the formulation. For a one-dimensional beam vibration [5], the weighted residual method was modified by including the boundary contribution through integration by parts. For the three-dimensional sound field, as shown in this paper, the first term on the left hand side of equation (3) can be expressed as follows [6]:

$$\int_V \phi_J(\mathbf{r})\nabla^2 p^{(N)}(\mathbf{r})\ \mathrm{d}v = \int_V p^{(N)}(\mathbf{r})\nabla^2\phi_J(\mathbf{r})\ \mathrm{d}v + \int_S \frac{\partial p^{(N)}(\mathbf{r})}{\partial n}\phi_J(\mathbf{r})\ \mathrm{d}s - \int_S \frac{\partial \phi_j(\mathbf{r})}{\partial n} p^{(N)}\mathrm{d}s. \tag{4}$$

The contribution of the movable boundaries to the sound field must be taken into account if the trial solution does not satisfy the natural boundary conditions. For this case, both trial solution (describing the pressure) and its gradient on the boundaries should be replaced by the corresponding natural boundary conditions. If the trial solution is expressed as:

$$p^{(N)}(\mathbf{r}) = \sum_{J=1}^{N} P_J\phi_J(\mathbf{r}), \tag{5}$$

where $\phi_J(\mathbf{r})$ are shape functions which satisfy the geometrical boundary conditions of the sound field, the N generalised co-ordinates P_J which define the amplitudes of the shape functions used can be obtained from the solution of equation (3) and correspond to the mode amplitudes in a modal expansion.

If the shape functions are taken to be the mode shapes of the rectangular enclosure with rigid walls:

$$\phi_J(\mathbf{r}) = \phi_{lmn}(\mathbf{r}) = \cos\frac{l\pi x}{L_x}\cos\frac{m\pi y}{L_y}\cos\frac{n\pi z}{L_z}, \tag{6}$$

equations (3) and (4) give rise to following equations for the generalised co-ordinate P_J

$$(k^2 - k_J^2)\Lambda_J P_J = -\int_S \phi_J(\mathbf{r})\frac{\partial p^{(N)}(\mathbf{r})}{\partial n}\ \mathrm{d}s - j\rho_o\omega\int_V \phi_J(\mathbf{r})q(\mathbf{r})\ \mathrm{d}v, \tag{7}$$

for $J = 1, 2, \ldots, N$, where the wavenumber of the Jth rigid mode is

$$k_J = k_{lmn} = \pi\sqrt{(l/L_x)^2 + (m/L_y)^2 + (n/L_z)^2}, \tag{8}$$

TABLE 1
Parameters of the plywood panels used for the analysis

ρ_p	550 kg/m^3
E_p	$7{\cdot}9 \times 10^9$ N/m^2
η_p	0·2
ν_p	0·35

and

$$\Lambda_J = \int_V \phi_J^2(\mathbf{r})\, \mathrm{d}v. \tag{9}$$

Because the non-rigid boundary conditions have a non-zero pressure gradient, equation (5) with rigid wall mode shapes $\phi_{lmn}(\mathbf{r})$ fails to predict the correct pressure gradient at the walls ($\phi_{lmn}(\mathbf{r})$ do not satisfy the natural boundary conditions of the enclosure). The gradient of the trial function in equation (7) must be replaced by the expression of the sound pressure gradient on the corresponding boundaries (i.e. $\partial p/\partial n = \partial p^{(N)}/\partial n$). In the frequency domain, the pressure gradient on a boundary is related to the normal velocity v_n of the boundary as:

$$\frac{\partial p}{\partial n}(\mathbf{r}) = -j\rho_o \omega v_n(\mathbf{r}). \tag{10}$$

In this analysis, the positive direction of the pressure gradient is towards the outside of the enclosure, and so for that of the normal velocity of the boundaries. The contribution of the surface vibration to the acoustic pressure in the enclosure can then be described by substituting equation (10) into equation (7). It becomes apparent that the pressure gradient on the non-rigid boundary surfaces will alter the characteristics of the rigid wall room. If the velocity on the boundary depends only on the local pressure according to the expression $v(\mathbf{r}) = \rho_o c_o \beta(\mathbf{r}) p(\mathbf{r})$, where $\beta(\mathbf{r})$ is the specific acoustic admittance of the boundary, then the surface is said to be locally reactive and a closed form solution for the mode amplitudes can be obtained fairly easily. In this paper the use of a generalised modal admittance function is considered to describe non-locally reacting boundaries, and the way in which a number of boundaries can contribute to this overall modal admittance function.

The boundaries of the enclosure, as shown in Figure 1, may be classified into the following four areas with total surface area $S = S_1 + S_2 + S_3 + S_4$: (a) S_1 includes three side walls ($x = 0$, $x = L_x$ and $y = L_y$) which are made up of 12 panel sound absorbers. Each absorber consists of absorption material, air gap and a plywood panel ($2{\cdot}1 \times 1{\cdot}05 \times 0{\cdot}02$ m^3). (b) S_2 refers to the floor ($z = 0$) which has a thin layer of carpet on the plywood panels backed by a rigid surface. (c) S_3 includes the ceiling and the front wall ($z = L_z$ and $y = 0$) which are made of 7 plywood panels without any damping treatment. Each panel has a size of $2{\cdot}1 \times 1{\cdot}05 \times 0{\cdot}02$ m^3. (d) S_4 describes the area of air leakage on the

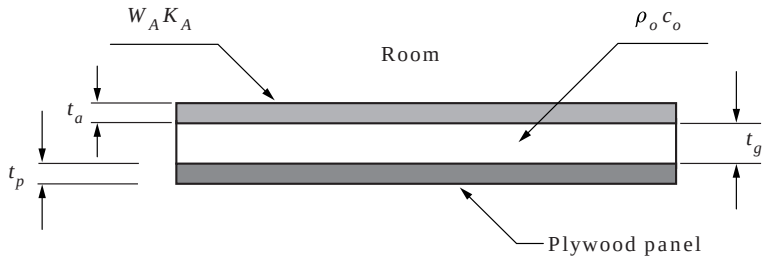

Figure 2. Configuration of one of the panel sound absorbers in boundary S_1.

boundaries. In particular there is an opening hole at $y=0$ ($0 \leqslant x \leqslant 0{\cdot}16$ m and $0 \leqslant z \leqslant 0{\cdot}10$ m).

2.2. CONTRIBUTION FROM PANEL ABSORBERS (S_1)

Figure 2 shows the configuration of one panel absorber (out of 12) in the boundary surface S_1. The parameters used to describe the absorbers are listed in Table 1. The porous mat shown in Figure 2 is described in terms of the complex specific acoustic impedance W_A and complex propagation constant K_A. They are functions of flow resistance R_1 of the mat and frequency [7]. For this analysis, the flow resistance R_1 is assumed to be 3000 Rayls/m.

In the low frequency range, the acoustic impedance at the back of the porous mat facing the Qth panel ($Q \in [1, 12]$) is the parallel combination of the specific acoustic impedance of the panel Z_{pQ} and the acoustic compliance of the air gap Z_g:

$$Z_{0Q} = \frac{Z_{pQ} Z_g}{Z_{pQ} + Z_g}, \tag{11}$$

where $Z_g = j(\rho_o c_o / \omega t_g)$. Similarly, the acoustic impedance on the surface of the mat in front of the Qth panel is the parallel combination of Z_{0Q} and the acoustic compliance of the mat Z_m:

$$Z_{1Q} = \frac{Z_{0Q} Z_m}{Z_{0Q} + Z_m} \tag{12}$$

where $Z_m = j(W_A / K_A t_a)$, and the acoustic compliances of the air gap and the mat are assumed to be the same for all the 12 panel absorbers.

The average acoustic impedance of a panel is used to represent Z_{pQ} of the plywood panels behind the porous mats. This average acoustic impedance is defined as the ratio between sound pressure p and averaged velocity of the panel. The modal expansion of the velocity of the Qth panel can be expressed as:

$$V_Q(\sigma) = \sum_{Q_Q=1}^{M_Q} V_{Q_Q} \psi_{Q_Q}(\sigma), \tag{13}$$

where $\psi_{Q_Q}(\sigma)$ is the shape function of the Q_Qth panel structural mode evaluated at location σ. As the plywood panels behind the porous mats are heavily

damped, the effect of the sound radiation loss of the panel is negligible. For this case, the modal velocity components of the panel vibration are:

$$V_{Q_Q} = -\frac{j\omega}{\rho^{(Q)}h^{(Q)}(\omega^2 - \omega_{Q_Q}^2 - j\eta_{Q_Q}\omega\omega_{Q_Q})\Lambda_{Q_Q}} \int_{S_{1Q}} p\psi_{Q_Q}(\sigma)\,\mathrm{d}s, \tag{14}$$

where $\rho^{(Q)}h^{(Q)}$ is the surface density of the panel, ω_{Q_Q} and η_{Q_Q} are respectively the natural frequency and modal loss factor of the Q_Qth mode. $\Lambda_{Q_Q} = \int_{S_{1Q}} \psi_{Q_Q}^2(\sigma)\,\mathrm{d}s$ and S_{1Q} is the surface of the Qth panel in boundary S_1.

The averaged surface velocity is:

$$\bar{V}_Q = \frac{1}{S_{1Q}} \int_{S_{1Q}} V_Q(\sigma)\,\mathrm{d}s, \tag{15}$$

which gives the volume velocity per unit area of the panel. For a uniform sound pressure on the panel surface, the acoustic impedance of the panel is defined as:

$$Z_{PQ} = \frac{p}{\bar{V}_Q} = -\frac{S_{1Q}}{\sum_{Q_Q=1}^{M_{Q_Q}} \dfrac{j\omega}{\rho^{(Q)}h^{(Q)}(\omega^2 - \omega_{Q_Q}^2 - j\eta_{Q_Q}\omega\omega_{Q_Q})\Lambda_{Q_Q}} \left[\int_{S_{1Q}} \psi_{Q_Q}(\sigma)\,\mathrm{d}s\right]^2}. \tag{16}$$

Therefore, the specific acoustic impedance Z_{1Q} on the surface of the mat supported by the Qth panel can be calculated using equations (16), (11) and (12). The boundary integration on S_1 in equation (7) for the Ith acoustic mode includes the contribution from the 12 panel sound absorbers in S_1:

$$\int_{S_1} \phi_1(\mathbf{r}) \frac{\partial p(\mathbf{r})}{\partial n}\,\mathrm{d}s = -j\rho_o\omega \sum_{Q=1}^{12} \sum_{I=1}^{N} \frac{C_{I,J}^{(Q)}}{Z_{1Q}} P_1, \tag{17}$$

where the coupling coefficient between the Ith and Jth rigid wall acoustic modes on the surface of S_{1Q} is:

$$C_{I,J}^{(Q)} = \int_{S_{1Q}} \phi_J(\sigma)\phi_I(\sigma)\,\mathrm{d}s. \tag{18}$$

If $I = J$, $C_{J,J}^{(Q)} = \int_{S_{1Q}} \phi_J^2(\sigma)\,\mathrm{d}s$ is thus a measure of the area of the Qth panel absorber, weighted by the magnitude of acoustic mode shape.

2.3. CONTRIBUTION OF A LOCALLY REACTIVE SURFACE (S_2)

The specific acoustic impedance of the thin carpet (thickness t_c) on a rigid floor surface can be modelled as:

$$Z_2 = -jW_C/\tan K_C t_c, \tag{19}$$

where W_C and K_C are respectively the complex specific acoustic impedance and complex propagation constant of the carpet. The expression of the boundary integration in equation (7) over S_2 for the Ith enclosure mode can be expressed as:

$$\int_{S_2} \phi_J(\mathbf{r}) \frac{\partial p(\mathbf{r})}{\partial n} \, \mathrm{d}s = -\frac{j\rho_o \omega}{Z_2} \sum_{I=1}^{N} C^{(2)}_{I,J} P_I, \tag{20}$$

where $C^{(2)}_{I,J}$ is the coupling coefficient between the Ith and Jth rigid wall acoustic modes over S_2.

2.4. CONTRIBUTION OF THE LIGHTLY DAMPED PANELS (S_3)

The boundary integration in equation (7) over S_3 describes the interaction between acoustical and structural modes. S_3 consists of *seven* individual panels ($P = 1, 2, \ldots, 7$; 5 of them on the surface $z = L_z$ and 2 on $y = 0$). Simply supported boundary conditions are assumed for this analysis. The modal expansion of the displacement of the Pth panel is:

$$W^{(P)}_P = \sum_{Q_P=1}^{M_P} W_{Q_P} \psi_{Q_P}(\sigma), \tag{21}$$

where W_{Q_P} and $\psi_{Q_P}(\sigma)$ are respectively the modal amplitude and shape function of the Q_pth mode of the Pth panel, and σ is again the location on the panel.

Using equation (10), the boundary integration in equation (7) on S_3 can be represented as:

$$\int_{S_3} \phi_J(\mathbf{r}) \frac{\partial p\mathbf{r}}{\partial n} \, \mathrm{d}s = \rho_o \omega^2 \int_{s_3} W_p \phi_J \mathbf{r} \, \mathrm{d}s = \rho_o \omega^2 \sum_{P=1}^{7} \sum_{Q_P} B_{Q_{P_J}} W_{Q_P}, \tag{22}$$

where W_p is the normal displacement of the boundary S_3 and $B_{Q_P,J}$ is the coupling coefficient between the Jth rigid wall acoustic mode and the Q_Pth panel mode of the Pth panel:

$$B_{Q_{P,J}} = \int_{S_3^{(P)}} \psi_{Q_P}(\sigma) \phi_J(\mathbf{r}) \, \mathrm{d}s. \tag{23}$$

As the mode shape of the panel is defined by the local co-ordinates of the panel, it is necessary to transfer the local co-ordinate into the co-ordinate of the enclosure to calculate the coupling coefficients.

For a simply supported panel with length $L^{(P)}_X$ and width $L^{(P)}_Y$, the mode shape functions are:

$$\psi_{Q_P}(\sigma) = \psi_{rs}(\sigma) = \sin \frac{r\pi x_{Q_P}}{L^{(P)}_X} \sin \frac{s\pi y_{Q_P}}{L^{(P)}_Y}, \tag{24}$$

where (x_{Q_P}, y_{Q_P}) are position variables in the local co-ordinates of the panel. Using the bending wave equation of a thin plate, the modal components of the Pth panel are described as:

$$(-\rho^{(P)}h^{(P)}\omega^2 + D^{(P)}k_{Q_P}^4 + j\eta_{Q_P}D^{(P)}k_{Q_P}^4)\Lambda_{Q_P}W_{Q_P}$$
$$= \int_{S_s^{(P)}} \psi_{Q_P}(\sigma)p^{(N)}\,\mathrm{d}s - \int_{S_3^{(P)}} \psi_{Q_P}(\sigma)p^{ext}\,\mathrm{d}s \tag{25}$$

for $Q_P = 1, 2, \ldots, M_P$, where

$$k_{Q_P}^4 = \pi^4\left[\left(\frac{r}{L_X^{(P)}}\right)^2 + \left(\frac{s}{L_Y^{(P)}}\right)^2\right]^2 \tag{26}$$

and η_{Q_P} is the loss factor of the Q_P mode, $\rho^{(p)}$ and $h^{(p)}$ are respectively the density and thickness of the Pth panel.

$$D^{(P)} = \frac{E_p(h^{(p)})^3}{12(1-v_p^2)} \quad \text{and} \quad \Lambda_{Q_P} = \int_{S_3^{(p)}} \psi_{Q_P}^2\,\mathrm{d}s.$$

In equation (25), p^{ext} is the external sound pressure on the surface of S_3.

In this analysis, equation (22) describes the contribution of the seven panels ($P = 1, 2, \ldots, 7$) and shows that $\sum_{P=1}^{7} M_P$ extra unknowns of the displacement components of the panels exist in equation (7). Equation (25) provides the same number of equations for the extra unknowns. By combining equation (7) and equation (25) and using the integration on the other boundaries (S_1, S_2 and S_4), the resultant equations are complete in the sense that the number of equations are equal to the number of unknowns.

The second integration on the right-hand side of equation (25) may include: (1) External driving force and sound pressure on the external surface of modally reactive boundaries. (2) Back pressure of sound radiation from the vibrating boundaries. The external driving force and sound pressure are often provided as the system input function for the analysis of sound transmission into the enclosure. The estimation of the back pressure of the sound radiation, however, depends upon the characteristics of the acoustic space to which the radiating surfaces face. The loss of vibrating energy in practical structures is usually dominated by their internal damping and effect of back pressure on the panel vibration is ignored in this analysis. Therefore, the contribution of the sound pressure on the external surface of the panel to the panel vibration is controlled by the external forcing pressure $p^{(force)}$:

$$p^{ext} \approx p^{(force)}. \tag{27}$$

2.5. CONTRIBUTION FROM AN AIR LEAK (S_4)

The contribution of the air leakage to the boundary integration in equation (7) can be described as:

$$\int_{S_4} \phi_J(\mathbf{r}) \frac{\partial p(\mathbf{r})}{\partial n} \, \mathrm{d}s = -\frac{j\rho_o \omega}{Z_4} \sum_{I=1}^{N} C_{I,J}^{(4)} P_I, \tag{28}$$

where $C_{I,J}^{(4)}$ is the coupling coefficient over S_4.

If one only considers the opening hole at $y = 0$ ($0 \leqslant x \leqslant 0{\cdot}16$ m) and $0 \leqslant z \leqslant 0{\cdot}10$), the acoustic impedance Z_4 can be obtained by modelling the opening as an air-piston:

$$Z_4 = (jM_T\omega + R_r/S_4), \tag{29}$$

where $M_T = \rho_o S_4 l_e$ and $R_r = (\rho_o c_o/2\pi) S_4^2 k^2$ are respectively the equivalent air mass and sound radiation impedance of the air piston. l_e is the equivalent thickness of the air piston.

3. PREDICTED TRANSFER RESPONSE OF THE RECTANGULAR ENCLOSURE

3.1. RESPONSE TO A SOUND SOURCE

The source strength of a point sound source located at (0, L_y,0) is described as:

$$q(\mathbf{r}) = Q_o \delta(x)\delta(y - L_y)\delta(z). \tag{30}$$

If a volume velocity of $Q_o = 1$ m^3/s is used, the corresponding sound pressure (e.g., at (L_x0, L_z)) can represent the acoustic transfer impedance. Using equation (30), the volume integration in equation (7) gives:

$$j\rho_o \omega \int_V \phi_J(\mathbf{r}) q(\mathbf{r}) \, \mathrm{d}v = j\rho_o \omega Q_o (-1)^m, \tag{31}$$

where m is the acoustic modal index in the Y direction (see equation (6)).

If the sound field is driven only by the internal acoustic sound source, equation (25) will give rise to an explicit expression for the modal amplitudes of the panels of S_3.

$$W_{Q_P} = -\frac{1}{\rho^{(p)} h^{(p)} \Lambda_{Q_P} (\omega^2 - \omega_{Q_P}^2 - j\eta_{Q_P}\omega\omega_{Q_P})} \sum_I B_{Q_P I} P_I, \tag{32}$$

where

$$\omega_{Q_P}^2 = \frac{D^{(p)} k_{Q_P}^4}{\rho^{(p)} h^{(p)}}.$$

Using the net specific acoustic admittance $\beta = \rho_o c_o / Z$ for each surface area, where Z is acoustic impedance of the surface, and using equations (17), (20), (22), (32) and (28), equation (7) can be re-written as:

$$(k^2 - k_J^2)\Lambda_J P_J - jk\sum_I \beta_I^{(1)} C_{I,J}^{(1)} P_I - jk\sum_I \beta^{(2)} C_{I,J}^{(2)} P_I$$

$$- jk\sum_I \beta^{(4)} C_{I,J}^{(4)} P_I - jk\sum_I \beta_{I,J}^{(3)} C_{I,J}^{(3)} P_I = -j\rho_o \omega Q_o (-1)^m, \tag{33}$$

where

$$\beta_I^{(1)} C_{I,J}^{(1)} = \rho_o c_o \sum_{Q=1}^{12} \frac{C_{I,J}^{(Q)}}{Z_{1Q}}, \tag{34}$$

$$\beta^{(2)} C_{I,J}^{(2)} = \rho_o c_o \frac{C_{I,J}^{(2)}}{Z_2}, \tag{35}$$

$$\beta_{I,J}^{(3)} C_{I,J}^{(3)} = \rho_o c_o \sum_{P=1}^{7} \sum_{Q_P} \frac{-j\omega B_{Q_P,I} B_{Q_P,J}}{\rho^{(P)} h^{(P)} (\omega^2 - \omega_{Q_P}^2 - j\eta_{Q_P}\omega\omega_{Q_P})\Lambda_{Q_P}}, \tag{36}$$

and

$$\beta^{(4)} C_{I,J}^{(4)} = \rho_o c_o \frac{C_{I,J}^{(4)}}{Z_4}, \tag{37}$$

Equation (33) describes the effect of the boundaries on the response of the sound field in terms of the modal coupling coefficients $\beta_{I,J}C_{I,J}$ among all the rigid wall acoustic modes. For the locally reactive boundaries, such as S_1, S_2 and S_4, $\beta_{I,J}$ describes the nature of sound absorption by the boundary materials while $C_{I,J}$ represents the geometrical coupling between the Ith and Jth rigid wall modes over the specific locally reactive boundary surfaces. For the modally reactive surface such as S_3, $\beta_{I,J}^{(3)}$ and $C_{I,J}^{(3)}$ shown in equation (36) cannot be separated as the sound absorption by the panel is due to the global coupling between the acoustical and structural modes and to the modal absorption of the structures.

Equation (33) also shows that the effect of boundaries on the sound field are through their modification of each individual co-ordinate (modal amplitude) of the rigid wall acoustic mode P_J. Qualitatively, P_J is directly modified by the boundaries through the following term:

$$\beta_{J,J} C_{I,J} = \beta_J^{(1)} C_{J,J}^{(1)} + \beta^{(2)} C_{J,J}^{(2)} + \beta_{J,J}^{(3)} C_{J,J}^{(3)} + \beta^{(4)} C_{J,J}^{(4)}. \tag{38}$$

The real part of $\beta_{J,J}C_{J,J}$ provides the modal damping and the imaginary part corresponds to the shift of natural frequency from that of rigid wall acoustic modes. The external "forcing term" includes not only the contribution from the sound source, but also that from the acoustical/acoustical coupling of the Jth mode with other modes.

3.2. RESULTS AND DISCUSSION

To explain the features of acoustical transfer impedance measured in the damped rectangular enclosure, the traditional approach is to introduce a specific

acoustic modal admittance $\beta_{J,J}$. For this case, the generalised co-ordinate can be expressed as

$$P_I = -\frac{j\rho_o \omega Q_o (-1)^m}{(k^2 - k_j^2)\Lambda_J - jk\beta_{J,J} C_{J,J}}, \tag{39}$$

where

$$C_{J,J} = \int_S \phi_{lmn}^2(\mathbf{r})\, \mathrm{d}s = 2(\gamma_m \gamma_n L_y L_z + \gamma_n \gamma_l L_z L_x + \gamma_l \gamma_m L_x L_y). \tag{40}$$

γ_l, γ_m, $\gamma_n = 1$ if l, m, $n = 0$ and γ_l, γ_m, $\gamma_n = 1/2$ if l, m, $n \neq 0$. The space-average response can be calculated by

$$\langle pp \rangle^* = \sum_{I=1}^{N} |P_I|^2 \frac{\Lambda_I}{V},$$

which is used to describe the space-average acoustic transfer impedance when $Q_o = 1$.

Several values of specific acoustic admittance were used for the best curve-fitting of the measured acoustic transfer impedance. Figure 3 shows the calculated acoustic transfer impedance, when a constant value of specific acoustic admittance, $\beta_{J,J} = 0{\cdot}067$, is used in equation (39). In this calculation the number of cavity modes is $l_{max} \times m_{max} \times n_{max} = 9 \times 11 \times 9 = 981$. Compared with the measured acoustic transfer impedance, a reasonable agreement can be found except at the low frequencies, in which case there is a difference of up to 20 dB. A better fit above 40 Hz could be obtained if $\beta_{J,J}$ was allowed to increase with frequency. If a negative imaginary value is arbitrarily included in the equivalent acoustic admittance (e.g. $\beta_{J,J} = 0{\cdot}067 - j0{\cdot}2$) to describe a mass controlled boundary reactance at low frequencies, some improvement in the prediction of the space-averaged impedance at some frequencies can be observed (see Figure 3). This suggests that a complex and frequency dependant value of the effective total admittance for each mode, β_{JJ}, can be used to describe some of the effects observed in practice, particularly at low frequencies.

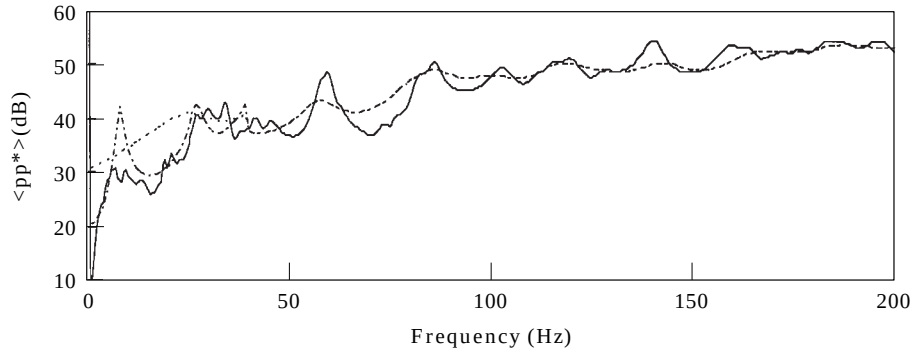

Figure 3. Average acoustic transfer impedance. Measured (———), predicted with $\beta_{J,J} = 0{\cdot}067$ (–·–·–), and with $\beta_{J,J} = 0{\cdot}067 - j0{\cdot}2$, $f < 40$ Hz, $\beta_{J,J} = 0{\cdot}067$, $f > 40$ Hz, (. . . . . .).

Following the theoretical analysis presented in this paper, one can calculate the value of the specific acoustic modal admittance $\beta_{J,J}$ corresponding to the actual boundary conditions as a function of frequency. As a first order approximation, the cross coupling between cavity modes due to the reactions of all the boundaries can be ignored. For this case, equation (38) is used only to calculate the complex term in the denominator of the sound pressure component in equation (39).

3.3. ABSORPTION BY PANEL ABSORBERS (S_1)

Observation of Figure 3 provides the following criteria for the identification of the boundary surfaces mainly responsible for the characteristics of the room response: (1) The real part of the specific acoustic modal admittance of the boundaries which are responsible for the sound absorption in the enclosure should be in the order of 0·07 in the frequency range above 40 Hz. (2) The imaginary part of the specific acoustic admittance of the boundary structures which determines the low frequency response of the enclosure should be in the order of 0·2 at the very low frequencies. (3) The acoustical/acoustical modal coupling coefficients $C_{J,J}$ give a measure of the required area for the sound absorption and the contribution to the modal coupling. Equation (40) shows that $7{\cdot}4\ \mathrm{m}^2 \leqslant C_{J,J} \leqslant 59{\cdot}2\ \mathrm{m}^2$ for the various shape functions used in this analysis.

When the specific acoustic impedance of the plywood panels behind the porous mats are included in the analysis, a large increase in the specific acoustic admittance may be found at the resonance frequencies of the volume displacement modes of the panels. Using equation (16) as the specific acoustic impedance of the panel for equations (11) and (12), the specific acoustic admittance on the surface of porous mats can be obtained. When simply supported mode shape functions are used, equation (16) can be simplified as:

$$Z_{PQ} = \frac{p}{V_Q} = -\left[\sum_{p,\,q=1,\,3,\,5,\,\ldots} 4\left(\frac{4}{pq\pi^2}\right)^2 \frac{j\omega}{\rho^{(Q)}h^{(Q)}(\omega^2 - \omega''_{p,\,q} - j\eta_{p,\,q}\omega\omega_{p,\,q})}\right]^{-1}. \quad (41)$$

Figure 4 shows the specific acoustic admittance of the porous mat backed by an air gap and then a plywood panel. In the calculation of Z_{pQ} in equation (41), five volume displacement modes of the panel ((1, 1), (1, 3), (3, 1), (1, 5) and (5, 1)) were used, but only the effect of the first (1,1) mode is apparent in Figure 4. Three panels with stiffness values ($0{\cdot}5E_p$, E_p, $1{\cdot}5E_p$), where E_p is the actual Young's modulus of the panels, were used to describe the effect of differences in panel parameters on the resonance frequencies of the modes. The behaviour of specific acoustic admittance shown in Figure 4 is very similar to that of traditional panel sound absorbers [8]. Figure 4 shows that the specific acoustic admittance is characterised by the resonance absorption of the first panel mode. As S_1 occupies half of the total surface area of the enclosure, this large resonance absorption at the low frequencies (10 to 60 Hz) will have a large influence on the acoustic transfer impedance in the corresponding frequency range. Above 60 Hz (up to 200 Hz), the real part of the acoustic admittance is

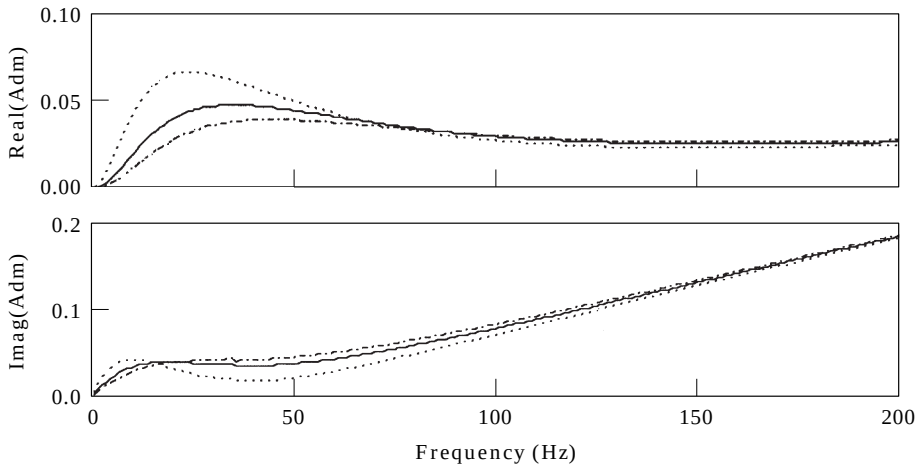

Figure 4. Specific acoustic admittance of the porous mat backed by an air gap and then a plywood panel of differing stiffness: $0{\cdot}5E_p$ (. . . . .), $E_p = 7{\cdot}9 \times 10^9$ N/m^2 (———) and $1{\cdot}5E_p$ (–·–·–).

also above 0·025 due to the off-resonance sound absorption of the panel supported mats. With a large area of sound absorption, one would expect that S_1 will also significantly affect the transfer impedance in the frequency range between 60 and 200 Hz. Because of the stiffness at the support of the panels, both real and imaginary acoustic admittance are very small at the very low frequencies (<10 Hz). Therefore, S_1 will not have a significant effect on the characteristics of the room at very low frequencies.

3.4. ABSORPTION BY LOCALLY REACTING SURFACE (S_2)

The porous mat used for the enclosure is described by the flow resistance and thickness ($R_1 = 3000$ Rayls/m, $t_a = 0{\cdot}025$ m). The specific acoustic admittance of the porous mat backed directly by a rigid surface and by an air gap ($t_g = 0{\cdot}025$ m) and then a rigid wall are calculated using equations (11) and (12). In the frequency range of interest (<200 Hz), the maximum values of the real part of the specific acoustic admittance for these two configurations are less than 0·015 and 0·018, respectively. At low frequencies, the positive imaginary values of the specific acoustic admittance for both cases are less than 0·05, which indicates that the stiffness controlled reactance of the materials is negligibly small. In addition, the acoustical/acoustical modal coupling coefficients on S_1 are also smaller than $C_{J,J}$ described in equation (40). In summary, the highly damped response of the sound field in this frequency range is not controlled by the mechanism of the sound absorption of the porous mat. For the same reason, the contribution of the thin carpet on S_2 to the low frequency sound absorption is also not significant.

3.5. ABSORPTION BY LIGHTLY DAMPED PANELS (S_3)

The interaction between one plywood panel on the $y = 0$ surface ($0 \leqslant x_{Q_1} \leqslant 1{\cdot}2$ m, $0 \leqslant z_{Q_1} \leqslant 2{\cdot}1$ m) is considered in the calculation of the room

TABLE 2

Resonance frequencies of the first 50 *rigid wall modes of the enclosure*

l	m	n	f_{lmn}	l	m	n	f_{lmn}
0	0	0	0	0	1	2	166·2
0	1	0	28·6	2	1	0	166·2
0	2	0	57·3	0	6	0	172·0
0	0	1	81·9	0	2	2	173·5
1	0	0	81·9	2	2	0	173·5
0	3	0	86·0	1	0	2	183·1
0	1	1	86·7	2	0	1	183·1
1	1	0	86·7	1	5	1	184·2
0	2	1	99·9	0	3	2	185·0
1	2	0	99·9	2	3	0	185·0
0	4	0	114·6	1	1	2	185·3
1	0	1	115·8	2	1	1	183·3
0	3	1	118·7	0	6	1	190·5
1	3	0	118·7	1	6	0	190·5
1	1	1	119·3	2	2	1	191·9
1	2	1	129·2	1	2	2	191·9
0	4	1	140·9	0	4	2	199·9
1	4	0	140·9	2	4	0	199·9
0	5	0	143·3	0	7	0	200·6
1	3	1	144·2	2	3	1	202·3
1	4	1	162·9	1	3	2	202·3
0	0	2	163·8	1	6	1	207·3
2	0	0	163·8	1	4	2	216·0
1	5	0	165·0	2	4	1	216·0
0	5	1	165·0	0	7	1	216·7

response. The indices and resonance frequencies of the first 15 panel modes (simply supported boundary conditions) and the first 50 cavity modes are listed in Tables 2 and 3. In the modelling, nine panel modes and 891 cavity modes were used.

With the variations in the panels' stiffness, boundary conditions and possible coupling between the panels, a large number of modes (more than 70) are expected to have natural frequencies in the frequency range of interest. Therefore, the consideration of the coupling with the seven plywood panels in S_3 can give some indicative results. Figure 5 shows the acoustic transfer impedance of the enclosure for panels with different stiffness ($0{\cdot}5E_p$, E_p and $1{\cdot}5E_p$, $\eta_{Q_p} = 0{\cdot}1$). The damping provided by the panel to the sound field is selective in narrow frequency bands. For example, the panel with stiffness E_p provides larger damping to the response around 30 Hz , while the panel with stiffness $1{\cdot}5E_p$ has larger sound absorption around 70 Hz. It can be observed from Figure 5 that the coupling between the simply supported panels in S_3 and the sound field is also not capable of providing much decrease of the room response at the low frequencies (<20 Hz) because the finite panel is in the stiffness controlled region below its first resonance frequency.

TABLE 3

Resonance frequencies of the first 15 *modes of a simply supported panel*

p	s	f_{ps} $0{\cdot}5E_p$	f_{ps} E_p	f_{ps} $1{\cdot}5E_p$
1	1	23·9	33·8	41·5
1	2	41·6	58·9	72·1
1	3	71·1	100·6	123·2
2	1	78·1	110·5	135·3
2	2	95·8	135·5	166·0
1	4	112·4	159·0	194·7
2	3	125·3	177·2	217·1
1	5	165·5	234·1	286·7
2	4	166·6	235·6	288·6
3	1	168·4	238·2	291·8
3	2	186·1	263·3	322·4
3	3	215·6	305·0	373·5
2	5	219·7	310·7	380·5
1	6	230·4	325·8	399·1
3	4	256·9	363·4	445·0

When all the modally reactive boundaries are included, the sound absorption by the modally reactive panels becomes significant. Together with the panel-mat surface, they appear to be the main sources of sound absorption in the frequency range from 60 to 200 Hz.

3.6. ABSORPTION BY AIR LEAKAGE ONLY (S_4)

The specific acoustic admittance of the 0·016 m^2 rectangular opening in the enclosure (from equation (29)) is shown in Figure 6. Because of the small area of the leakage, the contribution of the leakage to the acoustic damping is negligible. However, the mass controlled reactance is significant at the very low frequencies and increases the nature frequency of the cavity from 0 Hz. Because of the shift in the natural frequency, the response of the sound field is significantly reduced

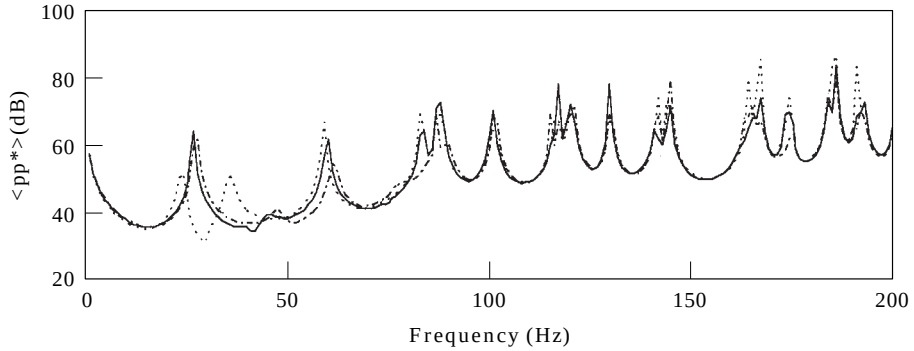

Figure 5. Acoustic transfer impedance of the enclosure with seven plywood panels of differing stiffness: $0{\cdot}5E_p$ (. . . . .), $E_p = 7{\cdot}9 \times 10^9$ N/m^2 (———) and $1{\cdot}5E_p$ (–·–·–).

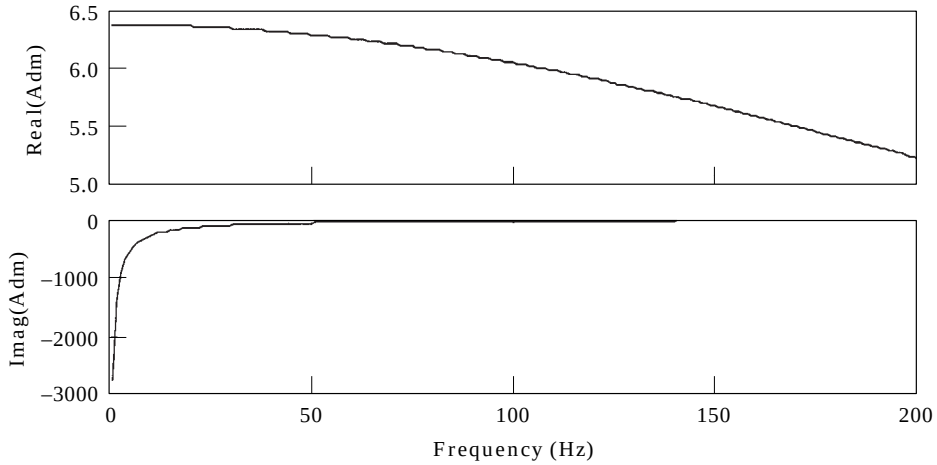

Figure 6. Specific acoustic admittance of the opening surface S_4 describing the air leakage.

at the very low frequencies. It can be shown that the air leakage of the cable hole decreases the magnitude of the transfer impedance of the enclosure at very low frequencies (below 10 Hz) because of the large mass controlled reactance. However, the averaged response at higher frequencies is not reduced significantly.

Because the imaginary part of the specific acoustical impedance of leakage is very large, the resonance frequency of the 0, 0, 0 acoustic mode is no longer zero due to the Helmholtz resonator formed by the inertance of the air in the opening and the compliance of the air in the cavity. This resonance frequency of this Helmholtz resonator can be estimated by

$$\omega_H = \sqrt{\frac{1}{C_A M_A}}, \tag{42}$$

where $C_A = V_o/\rho_o c_o^2$ is the acoustical capacitance of the enclosure volume V_o and $M_A = M_T/S_4^2$ is the acoustical mass of the opening hole, which corresponds to 9·5 Hz for the laboratory enclosure considered here.

3.7. CONTRIBUTION FROM ALL THE BOUNDARIES

In this analysis, the effect of boundary absorption on the acoustical transfer impedance is described by modal admittance (equations (38) and (39)). Figure 7 shows the admittance of the first acoustic mode (0, 0, 0), and contribution from each of the four boundaries. The peak values of the modal admittance at 42 and 108 Hz are contributed to by the resonance absorption of the lightly damped panels (S_3). The large admittance at the panel resonance has a significant effect on the room response when the corresponding structural resonance frequency is close to that of the room (see Figure 5, when panel stiffness is $0{\cdot}5E_p$). The admittance at off-resonances is dominated by the panel sound absorbers (S_1). Because of the small air leakage area, the contribution of S_4 to real($\beta_{0,0,0}$) is very small. However, the air leakage on S_4 has a significant contribution to

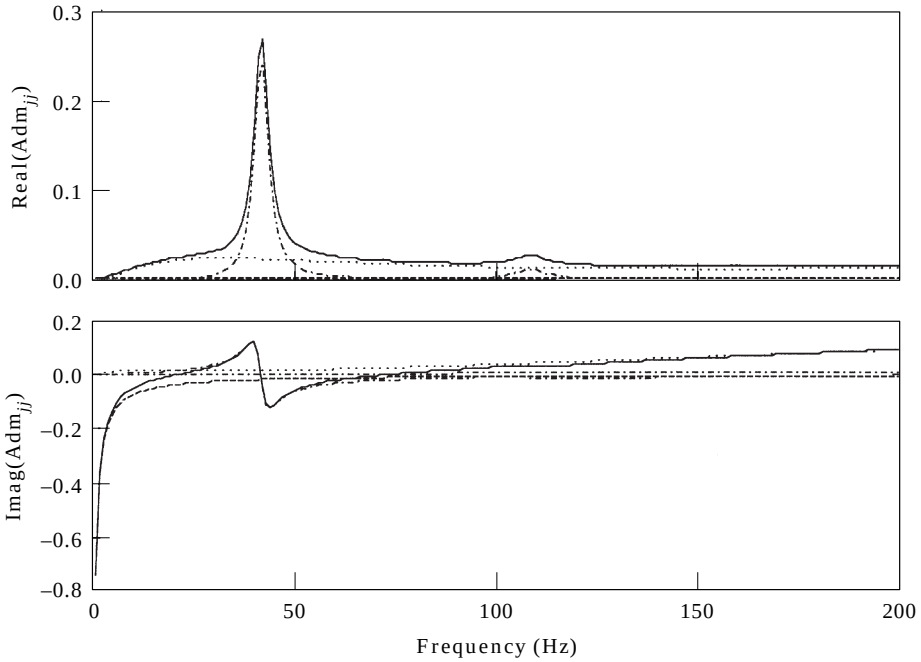

Figure 7. Admittance of acoustic mode (0, 0, 0): (———) and contributions from four surfaces: S_1 (. . . . .), S_2 (–·–·–), S_3 (–·–·–) and S_4 (– – – –).

imag($\beta_{0,0,0}$) at the low frequencies, which causes the shift of resonance frequency of mode (0, 0, 0) to the Helmholtz resonance frequency (equation (42)). The contribution of S_2 to $\beta_{0,0,0}$ is negligible.

The predicted average acoustical transfer impedance of the enclosure for each of the four surfaces are shown in Figure 8. The effect of boundary admittance on the acoustic transfer impedance has shown that three mechanisms of boundary absorption are at work in three frequency ranges. As summarised in Figure 9, the behaviour of the acoustic transfer impedance at very low frequencies (0–10 Hz) is controlled by the air leakage (S_4). Above the very low frequency range, the resonance absorption (10 to 60 Hz) of the panel-mats surface (S_1) starts to control the transfer impedance. Above 60 Hz, the coupling between the cavity modes and the panel modes distributed in S_3 provide certain damping to the sound field. Therefore, the interaction between the cavity modes with the modes in the panel-mat surfaces (S_1) and in the panels' structural modes of S_3 dominates the general feature of the acoustic transfer impedance above the very low frequency range.

Contributions from all the boundary surfaces were included in the final calculation of the space-average acoustic transfer impedance as shown in Figure 10. This shows that a reasonable prediction of the space-average transfer impedance of the enclosure can be made on the basis of estimation of the boundary properties for the specific acoustic modal admittance described in equations (38) and (34)–(37).

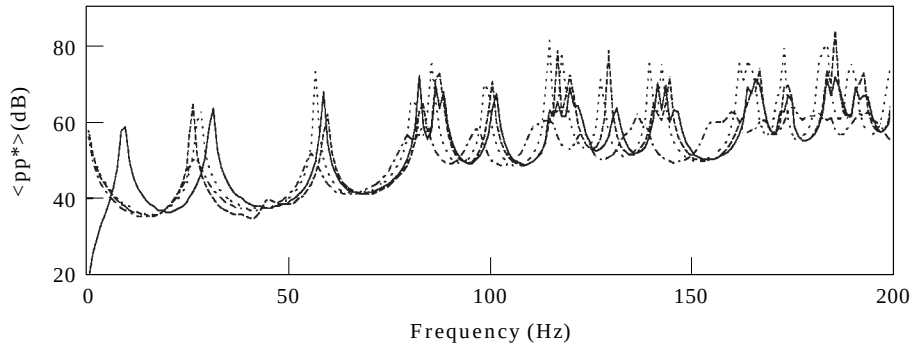

Figure 8. Predicted average acoustical transfer impedance of the enclosure for each of the four surfaces: S_1 (–·–·–), S_2 (. . . . .), S_3 (– – – –) and S_4 (———).

The major assumption in using equation (39) is that the cross coupling of the enclosure modes can be ignored. Previous analysis [9] has shown that when the specific acoustic impedance $Z/\rho_o c_o$ of the boundary of a one-dimensional tube is larger than about $15 \sim 20$, the cross coupling can be ignored. The estimated value of the specific acoustical admittance is about 0·067 in this case, which gives a value of $Z/\rho_o c_o = 15$, so that the assumption of uncoupled modes appears to be justified in this case.

4. HELMHOLTZ RESONANCE EFFECT OF THE COCKPIT IN THE HELICOPTER

The model described in the previous sections can be used to predict the acoustical response in the helicopter if the boundary and source conditions of the helicopter were available. However, in this section only the modelling of the Helmholtz resonance effect of the cockpit in the helicopter is considered by introducing the acoustic impedance of the resonator into equation (33). The results from this modelling may be used to explain the pronounced dip in the response at about 23 Hz (see Figure 12). A plan view of the helicopter used to take these measurements is shown in Figure 11. This dip in the impedance curve

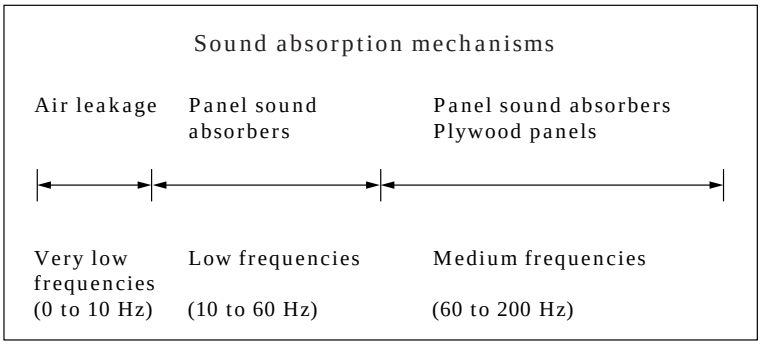

Figure 9. Effects of boundaries on the acoustic transfer impedance of the enclosure.

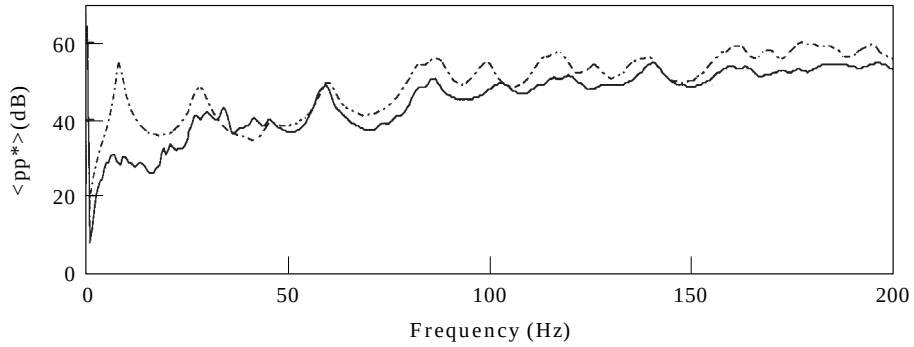

Figure 10. Average acoustical transfer impedance of the enclosure. Measured (———) and predicted considering the contributions of all the boundary surfaces (–·–·–).

is thought to be due to the effects of the Helmholtz resonator formed by the relatively narrow passage into the cockpit, approximately 0·7 m wide, 1·8 m high and with an effective length of 2 m, and the volume of air in the cockpit, approximately 3 m^3. The acoustic impedance of such a resonator can be written as

$$Z_r = R + j\omega L + \frac{1}{j\omega C}, \tag{43}$$

where R is the acoustic resistance of the resonator, which is assumed to be negligible here, L is the acoustic inertance, given by $L = \pi_o l'/S$ where l' is the effective length, S the cross-sectional area of the neck, and C is the acoustic compliance, given by $C = V/\rho_o c_o^2$, V being the volume of the resonator. The Helmholtz resonance frequency is given when the reactive part of equation (43) goes to zero and is equal to about 23 Hz for the neck and cavity dimensions given above. The acoustic impedance given by equation (43) can be divided by the characteristic impedance, $\rho_o c_o/S$, to give the specific acoustic impedance of the Helmholtz resonator, and if R is small, it can be seen that the specific

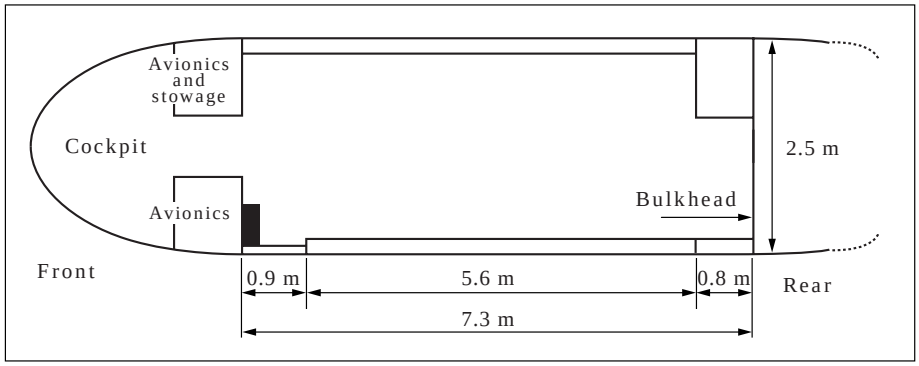

Figure 11. A plan view of the helicopter used for the measurements of acoustical transfer impedance.

acoustic impedance can fall well below the value of 15, which was mentioned above as the minimum value necessary to ensure that cross-coupling of the enclosure modes can be ignored.

To incorporate the effect of the Helmholtz resonator formed by the cockpit passage and volume into the model for the acoustic response of the passenger cabin, the specific acoustic admittance over the area of the passage can be taken to be

$$\beta_r = \frac{\rho_o c_o}{S Z_r} \tag{44}$$

but the cross coupling effects between the enclosure modes must be accounted for near the Helmholtz resonance frequency, when β_r is relatively large. These effects have been incorporated by rewriting equation (33) in matrix form as

$$\mathbf{K}\mathbf{p} - \mathbf{B}_r\mathbf{p} = \mathbf{q} \tag{45}$$

where the vector of principle co-ordinates (mode amplitudes) is

$$\mathbf{p} = [P_1,\ P_2, \ldots,\ P_N]^{\mathrm{T}}, \tag{46}$$

the vector of modal excitations for the corner acoustic source is

$$\mathbf{q} = j\rho_o\omega Q_o[1,\ -1, \ldots]^{\mathrm{T}}, \tag{47}$$

the matrix of wavenumbers is

$$\mathbf{K} = \begin{bmatrix} \Lambda_1(k^2 - k_1^2) & 0 & 0 & \ldots \\ 0 & \Lambda_2(k - k_2^2) & 0 & \ldots \\ . & . & & \\ & & & \Lambda_N(k - k_N^2) \end{bmatrix}, \tag{48}$$

and the matrix of terms due to the Helmholtz resonator is

$$\mathbf{B}_r = jk\beta_r \begin{bmatrix} C_{11} & C_{12} & . & . & . \\ C_{21} & C_{22} & & & \\ . & & . & & \\ . & & & . & \\ . & & & & C_{NN} \end{bmatrix}. \tag{49}$$

C_{jk} is given by equation (18) evaluated over the area of the cockpit passage. The effect of other boundaries can be taken into account by adding additional terms to $\mathbf{B}_r$ to include the effects of the other terms in equation (33) as described above. Unfortunately, a detailed model for the other boundaries, such as that used for the laboratory enclosure, was not available for the helicopter and so to illustrate the effect of the Helmholtz resonator the modal damping ratio,

$$\xi_J = \frac{c_o \beta_{JJ} C_{JJ}}{\omega_J V}, \tag{50}$$

was assigned the value $\xi = 0{\cdot}1$ for all the enclosure modes to account for the damping in the enclosure.

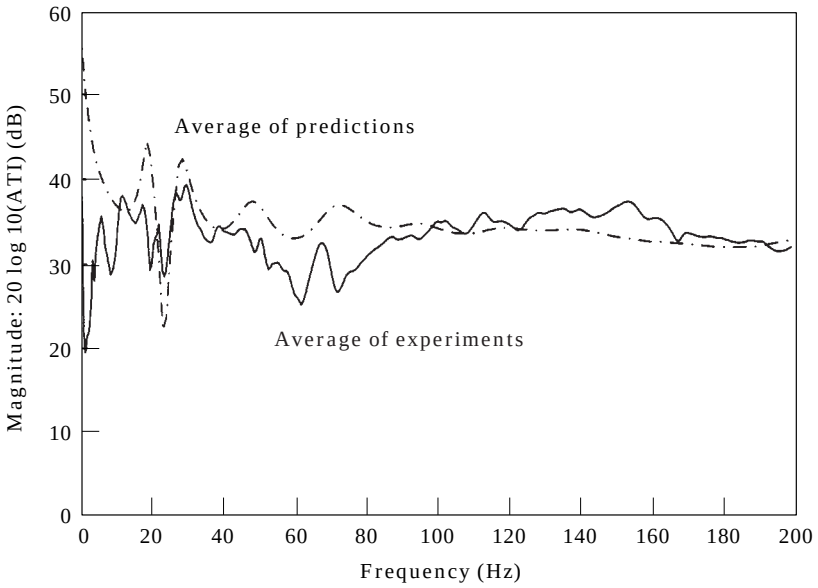

Figure 12. Average acoustical transfer impedance of the passenger cabin of EH101. Measured (———) and predicted (–·–·–).

Figure 12 shows the space arranged acoustic impedance measured in the helicopter and that calculated using the model outlined above. Although most of the response below 80 Hz has not been very accurately modelled, because the effects of the panel resonators and air leaks are being ignored in this simple model, the measured dip in the response at above 23 Hz is accurately predicted. Above about 80 Hz the space-average acoustic impedance is relatively uniform and its level is fairly accurately predicted by the simple modal model with a modal damping ratio of 0·1.

5. CONCLUSIONS

Using the modified method of weighted residual, the response of an enclosed sound field can be described by a set of admissible functions. When the admissible functions are the eigenfunctions of the rigid wall enclosure, similar modal equations to those developed by Dowell *et al.* were obtained. However, the formulation of the sound pressure response allows the use of other admissible functions for fast convergence of the results [10]. A formula (equation (33)) was derived to predict the response of the enclosure to the excitation of sound source. In equation (33), the contribution of all the boundaries are modelled in the same format. The contribution of the boundaries to the sound field response is through the modification of the modal amplitudes of rigid wall acoustic modes by changing the characteristics of the modes and by introducing modal coupling forcing terms.

When the cross coupling between the cavity modes is ignored, the specific acoustical modal admittance, β_{JJ}, is related to the properties of the boundary

structures by equations (34)–(38). It becomes obvious that $\beta_{J,J}$ is both frequency and modally dependent. A general model is developed to predict the acoustic transfer impedance of the enclosure with both locally and modally reactive boundaries. If the estimated specific impedance of the boundary surface is in the order of 20, equations (38) and (39) can be used for the prediction. If the estimated specific impedance is very small, such as when a Helmholtz resonator is coupled to the enclosure, cross mode coupling should be considered. For this case a matrix extension of equation (33) should be used.

This model was used to successfully predict the general features of the acoustic response of both a helicopter passenger cabin and a laboratory enclosure. A more detailed modelling of the low frequency damping mechanisms in the laboratory enclosure was possible and these were found to be dominated by: (1) At very low frequencies, the air leakage at the cable opening hole and panel joints contribute significantly to the acoustic transfer impedance. The contribution of the air leakage with a small opening area is mainly through the mass reactance in increasing the original cavity resonance frequency from 0 Hz to the resonance frequency described by equation (42). (2) The resonance absorption of the panel-mat surface significantly controls the low frequency behaviour of acoustic transfer impedance (10 to 60 Hz). (3) Structural/acoustical coupling between the panel modes and the cavity modes also significantly attenuates the resonance response shown in acoustic transfer impedance. Together with the off-resonance sound absorption of the panel-mat surfaces, they dominate the characteristics of the acoustic transfer impedance in the medium frequency range (60 to 200 Hz).

The Helmholtz resonance effect of the cockpit in the helicopter is also included in the model. The measured dip at about 23 Hz in the space-average acoustic impedance inside the passenger cabin of the helicopter is accurately predicted.

ACKNOWLEDGMENTS

This work was conducted when the first author was on his study leave from the Department of Mechanical and Materials Engineering, University of Western Australia, Nedlands, WA 6907, Australia. Financial support from UWA for his study leave is gratefully acknowledged. The helicopter measurements were taken as part of the CEC project AER2-CT92-0046 RHINO, and the support of the EC and the other partners in this project, particularly GKN-Westland Helicopters, is gratefully acknowledged.

REFERENCES

1. C. C. BOUCHER, S.J. ELLIOTT and K.-H. BAEK 1996 *Proceedings of Internoise* 96, 1179–1182. Active control of helicopter rotor tones.
2. S. J. ELLIOTT, C. C. BOUCHER and K.-H. BAEK 1997 *Proceedings of Innovations in Rotorcraft Technology, Royal Aeronautical Society Conference, London*, 15.1–15.6. Active control of rotorcraft interior noise.

3. K.-H. BAEK 1996 *PhD Thesis, University of Southampton*. Non-linear optimisation problems in active control.
4. D. A. DOWELL, G. F. GORMAN, III and D. A. SMITH 1977 *Journal of Sound and Vibration* **52**, 519–542. Acousto-elasticity: general theory, acoustic natural modes and forced response to sinusoidal excitation, including comparisons with experiment.
5. L. MEIROVITCH and P. HAGEDORN 1994 *Journal of Sound and Vibration* **178**, 227–241. A new approach to the modelling of distributed non-self adjoint systems.
6. P. M. MORSE and K. U. INGARD 1986, *Theoretical Acoustics*. Princeton, NJ: Princeton University Press. See p. 320.
7. D. A. BIES and C. H. HANSEN 1980 *Applied Acoustics* **13**, 357–391. Flow resistance information for acoustical design.
8. R. D. FORD and M. A. MCCORMICK 1969 *Journal of Sound and Vibration* **10**, 411–423. Panel sound absorbers.
9. J. PAN 1994 *Journal of Acoustical Society of America* **96**, 2141–2144. A second note on the prediction of sound intensity.
10. J. PAN 1999 *Journal of Acoustical Society of America* **105**, 560–562. A third note on the prediction of sound intensity.